Analysis of absorbed dose in radioimmunotherapy with 177Lu-trastuzumab using two different imaging scenarios

Original article

Nuclear Medicine Communications

Analysis of absorbed dose in radioimmunotherapy with ^{177}Lu-trastuzumab using two different imaging scenarios: a pilot study

Amit Nautiyal[a,c], Ashish K. Jha[a,c], Sneha Mithun[a,c], Bhakti Shetye[a,c], Mythili Kameswaran[a,c], Sneha Shah[a,c], Venkatesh Rangarajan[a,c] and Sudeep Gupta[b,c]

Objectives **Internal organ dosimetry is an important procedure to demonstrate the reliable application of ^{177}Lu-trastuzumab radioimmunotherapy for human epidermal growth factor receptor-positive metastatic breast cancers. We are reporting the first human dosimetry study for ^{177}Lu-trastuzumab. Another objective of our study was to calculate and compare the absorbed doses for normal organs and tumor lesions in patients before radioimmunotherapy with ^{177}Lu-trastuzumab using two different imaging scenarios.**

Methods **Eleven patients (48.27 ± 8.95 years) with a history of metastatic breast cancer were included in the study. Postadministration of ^{177}Lu-trastuzumab (351.09 ± 23.89 MBq/2 mg), acquisition was performed using planar and hybrid imaging scenarios at 4, 24, 72 and 168 h. Single-photon emission computed tomography/computed tomography imaging was performed at 72 h postinjection. Acquired images were processed using Dosimetry Toolkit software for the estimation of normalized cumulated activity in organs and tumor lesions. OLINDA/EXM 2.0 software was used for absorbed dose calculation in both scenarios.**

Results **Significant difference in normalized cumulated activity and the absorbed dose is noted between two imaging scenarios for the organs and tumor lesions ($P < 0.05$). Mean absorbed dose (mGy/MBq) estimated from heart, lungs, liver, spleen, kidney, adrenal, pancreas and colon using planar and hybrid scenarios were 0.81 ± 0.19 and 0.63 ± 0.17; 0.75 ± 0.13 and 0.32 ± 0.06; 1.26 ± 0.25 and 1.01 ± 0.17; 0.68 ± 0.22 and 0.53 ± 0.16; 0.91 ± 0.3 and 0.69 ± 0.24; 0.18 ± 0.04 and 0.11 ± 0.02; 0.25 ± 0.22 and 0.09 ± 0.02 and 0.75 ± 0.61 and 0.44 ± 0.28, respectively.**

Conclusions **On the basis of our dosimetric evaluation, we concluded that radioimmunotherapy with ^{177}Lu-trastuzumab is well tolerated to be implemented in routine clinical practice against HER2 positive metastatic breast cancer. Liver is the main critical organ at risk. Hybrid scenario demonstrated significantly lower absorbed doses in organs and tumors compared to the multiplanar method.** ***Nucl Med Commun*** **42: 1382–1395**

Nuclear Medicine Communications 2021, **42**:1382–1395

Keywords: HER2, hybrid dosimetry, ^{177}Lu-trastuzumab, planar dosimetry, radioimmunotherapy, radionuclide therapy

[a]Department of Nuclear Medicine and Molecular Imaging, Tata Memorial Centre, Parel, [b]Department of Medical Oncology, Advanced Centre for Treatment, Research and Education in Cancer (ACTREC) and [c]Homi Bhabha National Institute, Mumbai, Maharashtra, India

Correspondence to Venkatesh Rangarajan, MBBS, DRM, DNB, MNAMS, Department of Nuclear Medicine and Molecular Imaging, Tata Memorial Hospital, Tata Memorial Centre, Dr Ernest Borges Rd, Parel, Mumbai, Maharashtra 400012, India
Tel: +91 9969014183; e-mail: drvrangarajan@gmail.com

Received 4 April 2021 **Accepted** 16 July 2021

Introduction

Human epidermal growth factor receptor-2 (*HER2*) is a gene that is overexpressed in 10–34% of breast cancers [1,2]. The treatments of primary breast tumor using various treatment strategies have proven to be effective. Radiolabelled mAb has been explored in radioimmunotherapy for the treatment of metastatic diseases [3]. Trastuzumab is a clinically approved mAb for the treatment of *HER2* expressing metastatic breast cancers [4]. To deliver the appropriate therapeutic dose, trastuzumab has been used as a carrier in targeted radionuclide therapy (RNT) for targeting *HER2* positive lesions [5–7].

The lanthanide ^{177}Lu is a lower energy beta emitter with short-range in tissue, which induces lower toxicity to normal tissue. Moreover, ^{177}Lu is a gamma emitter, $E\gamma = 208$ keV (11.1%), 113 keV (6.6%), which makes it ideal for imaging-based dosimetric calculations required for treatment monitoring and response during therapy. Previous research works have demonstrated the feasibility of ^{177}Lu-trastuzumab for radioimmunotherapy of *HER2* positive breast cancers [8–10]. However, due to the slower clearance rate of mAb from the blood pool and liver, considerable risk can be associated with radioimmunotherapy mainly because of radiation toxicity to normal tissues [11]. To avoid such side effects, individualized

0143-3636 Copyright © 2021 Wolters Kluwer Health, Inc. All rights reserved. DOI: 10.1097/MNM.0000000000001472

internal organ dosimetry is important with consideration of factors influencing dosimetry results [12,13].

Internal dosimetry using Medical Internal Radiation Dose formalism is most often performed by assessment of cumulative activity and absorbed dose in organs using region of interest (ROI)-based estimation from multiple planar whole-body scans [14]. In 2D scintigraphy, certain factors affect the accurate estimation of ROI activity, resulting in significant under or overestimation of absorbed dose from target organs [15–17]. However, three-dimensional (3D) single-photon emission computed tomography/computed tomography (SPECT/CT) was found to be useful in improving dosimetry accuracy [18–22]. The use of SPECT/CT in all imaging time points makes dosimetry a tedious and time-consuming process that is practically difficult to be implemented in routine clinical practice [23]. Therefore, to overcome this problem, the concept of hybrid dosimetry is introduced which is a combination of multiple whole-body planar images and single SPECT/CT [22,24,25].

Some biodistribution studies have been performed on animals as well as inpatients. However, no specific dosimetry reports are available in humans with ^{177}Lu-trastuzumab. We performed a dosimetry study aimed to estimate the absorbed doses for normal organs and tumor lesions in patients who will undergo radioimmunotherapy with ^{177}Lu-trastuzumab using two different imaging scenarios and compare them.

Materials and methods

Patients selection

Eleven female patients (48.27 ± 8.95 years, range 37–64) with a history of metastatic breast cancer were referred between November 2019 and March 2020 for radioimmunotherapy with ^{177}Lu-trastuzumab were retrospectively studied. This is a retrospective analysis of a prospective study approved by the institutional review board and informed consent was obtained from all patients. Inclusion criteria of the study were, histologically proven breast cancer patients with *HER2* protein scores of 3+ and normal blood cells counts including normal cardiac ejection fraction. Before pretherapeutic dosimetry imaging, all patients were slowly injected intravenously with a diagnostic dose of ^{177}Lu-trastuzumab (351.09 ± 23.89 MBq/2 mg) together with a cold injection of trastuzumab (20 mg).

Preparation and radiolabeling of CHX-A″-DTPA ([(R)-2-Amino-3-(4-isothiocyanatophenyl)propyl]-trans-(S,S)-cyclohexane-1,2-diamine-pentaacetic acid)-trastuzumab conjugate

The preparation technique as described by Kameswaran *et al.* [10] was used in this study. All preparations were carried out in a sterile apyrogenic manner. The radiochemical and chemical purity analysis was performed using both HPLC (Synthra GmbH) and instant thin layer chromatography (Eckert & Ziegler, Berlin, Germany).

Acquisition

Image acquisition was performed using a SPECT/CT system (Discovery NM/CT 670 pro; GE Healthcare, Haifa, Israel) at four different time points. This system comprises GE Optima CT 540 with 16 slice CT configuration. Whole-body planar scintigraphy was performed at 4, 24, 72 and 168 h postinjection of ^{177}Lu-trastuzumab. To minimize acquisition variability among patients, all set of images were acquired with minimum deviation of time for each time points using the same SPECT/CT system. SPECT/CT imaging of thorax, abdomen and pelvis was performed at 72 h postinjection. Image acquisition and reconstruction parameters were the same for all patients. Detailed planar, SPECT and CT acquisition parameters are mentioned in Table 1.

Calibration factor

The calibration factor was estimated in compliance with vendor recommendations. The calibration factor was entered manually to convert ROI or volume of interest (VOI) counts into activity. In this measurement, a petri dish was filled with the solution of ^{177}Lu (92.5 MBq) and saline. Camera sensitivity was estimated by the formula

$$\text{Sensitivity} = \frac{n/t}{a/d} \quad (1)$$

where n = number of counts stored in pixel, d = decay correction factor, t = total acquisition time and a = administered activity.

Image processing

Acquired images were processed using Dosimetry Toolkit software (DTK; GE Healthcare) [26] for the estimation of normalized cumulated activity in heart, lung, liver, spleen, kidney and liver tumor lesions. The normalized cumulated activity was calculated with multiplanar imaging scenario and hybrid scenario using multi whole-body planar images in addition to single SPECT/CT. In both imaging scenarios, 'Preparation for dosimetry toolkit express' application was used for raw data reconstruction and registration of whole-body planar images and SPECT/CT. Manual ROI tool and semiautomatic VOI segmentation tool were used for defining organs and tumors in the 2D and 3D scenarios, respectively. In planar whole-body images, threshold-based (10%) whole body ROI was contoured at 72 h reference image and thereafter ROI was projected over remaining whole-body images. Similarly, organ ROI is contoured manually by experienced Nuclear Medicine Physicist on 2D planar image and semiautomated method on 3D SPECT images with a 30% threshold. Organ ROIs in planar images are represented in Fig. 1a. The input parameters used to generate the time-activity curve and mono-exponential fitting are patient demographics, injected activity and system

Table 1 Acquisition parameters for planar and single-photon emission computed tomography/computed tomography examination

Collimator	MEGP
Collimator and energy window selection	
Energy window	113 keV ± 10 % and 208 keV ± 10 %
Scatter window	79.1–101.7 keV, 124.3–146.9 keV and 146–187.3 keV
Planar	
Table speed	8 cm/min
Zoom	1
Matrix size	256 × 1024
Image time postinjection (h)	4, 24, 72, 168
Pixel size (mm)	2.2
SPECT	
Bed positions	2
Acquisition mode	Step and shoot
Matrix size	128 × 128
No of projections	60
Time per view (s)	30
Angular increment (degree)	6
Reconstruction (iterations and subsets)	OSEM (2 and 10)
Image time point postinjection (h)	72
Voxel size (mm^3)	1.8
CT	
KVp	120
Mas	70
Slice thickness (mm)	3.75
Tube rotation time (s)	0.8
Matrix size	512 × 512
Pitch	1.37
Reconstruction	ASiR
Voxel size (mm^3)	0.75

ASiR, adaptive statistical iterative reconstruction; CT, computed tomography; MEGP, medium energy general purpose; OSEM, ordered subset expectation maximization; SPECT, single-photon emission computed tomography.

Fig. 1

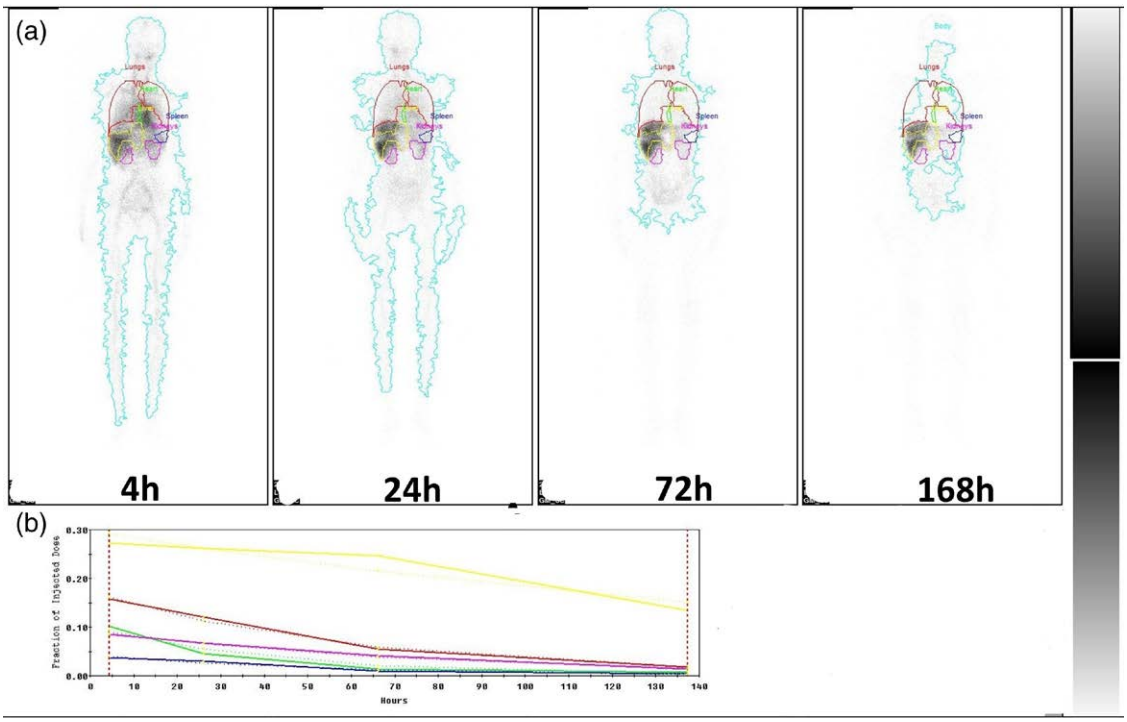

Representation of final result of Dosimetry Toolkit in hybrid scenario. (a) Demonstration of sequential GM and SC images of a patient with ROI 4, 24, 72 and 168 h postinjection(b) Fitting of curves for organ ROIs; heart (green); lungs (red); liver (yellow); spleen (blue) and kidneys (violet). ROI, region of interest.

sensitivity. This curve was used to estimate the uptake and normalized cumulated activity (Fig. 1b). DTK analysis report shows the percentage of injected dose (ID%) in source organ against each imaging time point, which was estimated using the following formulae:

$$\%\mathrm{ID}\ (t) = \frac{A_s}{A_i} \times 100 \tag{2}$$

and

$$A_s(t) = \frac{\mathrm{cpm}_s}{k} \tag{3}$$

where A_s is an activity in source organ at time t postinjection; A_i is injected activity in uCi; cpm_s is counts per minute of source organ at time t and k is the sensitivity of the system in cpm/uCi.

Similarly, normalized cumulated activity (Γ) in uCi.h/uCi was assessed using the following formula:

$$\Gamma = \frac{\tilde{A}}{A_0} \tag{4}$$

where $\tilde{A}$ is cumulated activity in organ, tumor lesion or remainder body and A_0 is total administered activity. The normalized cumulated activity in the remainder of the body was estimated as the difference between normalized cumulated activity in the total body and the sum of normalized cumulated activity in the heart, lungs, liver, spleen, kidneys and tumor lesions.

Planar scenario

In this scenario, scatter corrected geometric mean images from anterior and posterior projections are automatically computed from multiple whole-body scintigraphic images. Using 72 h whole body image as a reference image, all resulting images were co-registered to this time point. Threshold ROIs for all whole-body images were automatically stipulated by DTK. For organs and liver tumor lesions, ROIs were manually defined for the third imaging time point with the 2D ROI tool. During delineation of the whole liver, tumor ROI was performed first which was automatically subtracted from healthy liver ROI. After validation, all these ROIs were automatically propagated to the rest of the images of different time points. For misregistered internal organs or tumor lesions, ROIs were manually adjusted. Background correction was performed for each organ and tumor lesion. Depending on the location of the organ or tumor ROI, corresponding background ROI was generated automatically on either the left or right side. Background correction was performed by subtracting the organ ROI counts from weighted background counts. Background ROI parameters, that is, spacing, width, weightage as adjusted using background ROI tool under DTK. The weightage (w) was modified as described by Buijs *et al.* [27]

$$w = 1 - \frac{T_{\mathrm{organ}}}{T_{\mathrm{body}}} \tag{5}$$

The thickness of the organ (T_{organ}) and body (T_{body}) in the anterior–posterior direction was estimated from CT.

Hybrid scenario

Here, we combined multiple sets of whole-body scans with a single SPECT/CT acquired at 72 h. Preprocessing of the image is similar to the planar scenario. As per software recommendations, 'preparation for dosimetry toolkit express' was used for SPECT image reconstruction followed by the creation of planar and CT data with the same pixel and matrix size (256 × 256). In image reconstruction, SPECT data were corrected for motion, scatter, attenuation and resolution recovery. Thereafter, registration of planar image and maximum intensity projection (MIP) SPECT image was presented and matched using DTK. In a hybrid scenario, organs or tumor lesions are initially delineated on SPECT/CT images (Fig. 2a and b) and thereafter projected over the whole body planar images of all time points. This was done to remove superimposed regions or organ structures from ROIs (e.g. liver and right kidney) and subsequent correction of overlapping compartments from 2D planar images. All overlapping organ volumes were automatically removed from all planar images. Mean uniformly distributed radioactivity concentration in SPECT VOI was used as a substitution for the correction of activity from the removed volume of an organ (Fig. 2c). The scaling of planar data to SPECT activity concentration at 72 h was done using:

$$A_{\mathrm{H}}(t) = \frac{A_P(t)}{A_P(t_{\mathrm{SPECT}})} \times \frac{A_{\mathrm{SPECT}}(t_{\mathrm{SPECT}})}{R} \tag{6}$$

where $A_{\mathrm{H}}(t)$ = hybrid activity concentration at time t, $A_{\mathrm{P}}(t)$ = planar activity concentration at time t, $A_{\mathrm{P}}(t_{\mathrm{SPECT}})$ = activity concentration in the planar image acquired at time t_{SPECT} (72 h postinjection), $A_{\mathrm{SPECT}}(t_{\mathrm{SPECT}})$ = activity concentration in SPECT image acquired at time t_{SPECT} (72 h postinjection) and R = recovery coefficient obtained from SPECT VOI.

Above hybrid activity concentration at different time points was used for the calculation of the time-activity curve. We used semiautomatic and manual VOI tools for SPECT and CT image segmentation, respectively. During delineation of the whole liver, tumor VOI was performed first which was automatically subtracted from healthy liver VOI. Organ volumes were

Fig. 2

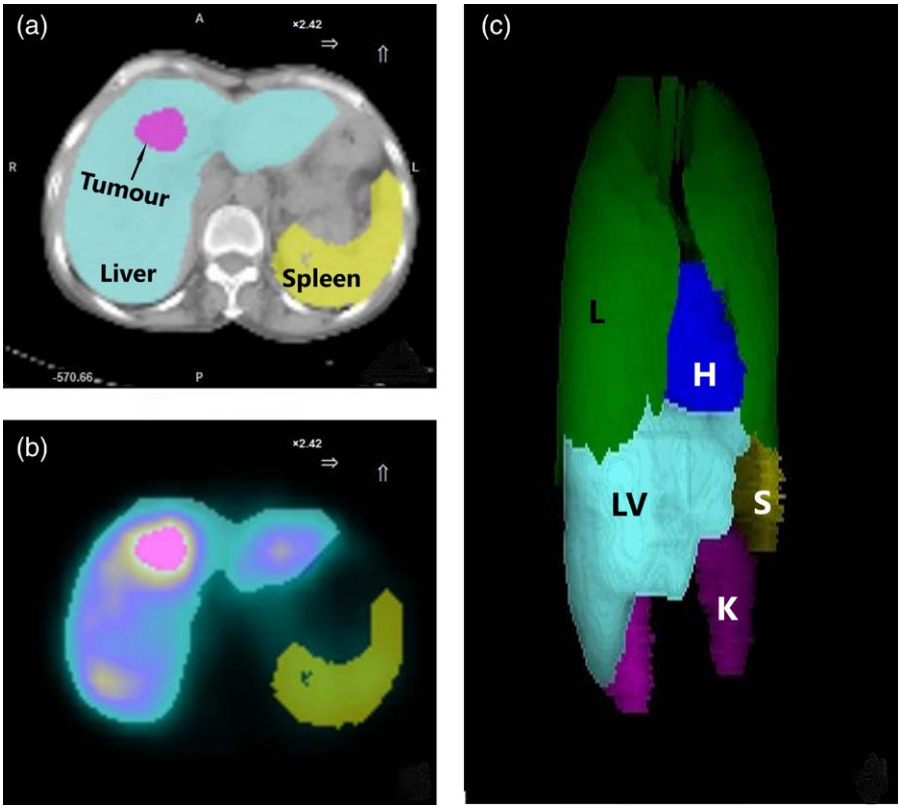

Example of a countered VOI in hybrid scenario 72 h postinjection(a) Delineation of liver, spleen and tumor lesion in 3D CT image. (b) Delineation of liver, spleen and tumor lesion in transaxial SPECT image. (c) 3D image segmentation of heart (H), lungs (L), liver (LV), spleen (S) and kidneys (K) for correction of overlapping regions and volume estimation. VOI, volume of interest.

estimated using a 3D MIP image generated from the same SPECT/CT images acquired in a hybrid scenario (Fig. 2c).

Dose estimation

The OLINDA/EXM 2.0 software [28] was used for absorbed dose estimation from organs. The main input parameters required for dose estimation (mGy/MBq) are normalized cumulated activity of organs and remainder body (obtained from DTK), radionuclide selection and organ masses. Organ masses were estimated using measured organ volume on CT and standardized organ densities [29]. Organ dose (D) was estimated according to the following formula:

$$D = N \times DF \tag{7}$$

where N is the number of disintegrations in the source organ and DF is the dose factor which is given by:

$$\mathrm{DF} = \frac{k\sum_i n_i E_i \varphi_i w_R}{m} \tag{8}$$

where k is unit conversation constant (Gy-kg/MBq-s-MeV or rad-g/mCi-h-MeV), n is the number of emissions with energy E, i represent the ith type emission, E is energy per emissions, φ is absorbed fraction, w_R is radiation weighting factor and m is organ mass.

Additionally, the unit density sphere model integrated into OLINDA/EXM 2 [30,31] was used for absorbed dose estimation in liver tumor lesions. Volumes of tumor lesions were estimated using CT, whereas the density of lesions was considered similar to the liver. In this model, precalculated S values for ^{177}Lu were defined for different spheres of different mass from 0.01 to 6000 g.

Statistical analysis

The SPSS software 64-bit edition (IBM Corporation, Armonk, New York, USA) was used for all statistical analyses. All parameters were denoted as mean ± SD, median, IQR and range. Organ and tumor normalized cumulated activity and absorbed dose per injected activity estimated by two imaging scenarios were tested for significance using a nonparametric Wilcoxon signed-rank test (P value < 0.05). Bland and Altman (B&A) plot was used to derive the limit of agreement (95% CI) between

estimates obtained using planar and hybrid imaging scenarios.

Results

Organ mass (g), organ normalized cumulated activity and remainder body normalized cumulated activity estimated for dosimetry in our study are mentioned in Tables 2 and 3. The mean absorbed dose per injected activity (DpA) (mGy/MBq) to heart, lungs, liver, spleen, kidneys, adrenal, pancreas and colon in planar scenario were 0.81 ± 0.19, 0.75 ± 0.13, 1.26 ± 0.25, 0.68 ± 0.22, 0.91 ± 0.31, 0.18 ± 0.04, 0.25 ± 0.22 and 0.75 ± 0.61, respectively. Similarly average absorbed dose per injected activity to heart, lungs, liver, spleen, kidneys, adrenal, pancreas and colon in hybrid scenario were 0.63 ± 0.17, 0.32 ± 0.06, 1.01 ± 0.17, 0.53 ± 0.16, 0.69 ± 0.24, 0.11 ± 0.02, 0.09 ± 0.02 and 0.44 ± 0.28, respectively. Details of absorbed doses are mentioned in Table 4. The average whole-body dose received by the patients in our study was 0.163 mGy/MBq. Average time points of 4, 24, 72 and 168 h imaging were 4.23 ± 0.47 h, 24.23 ± 0.61 h, 71.48 ± 1.11 h and 167.56 ± 1.70 h, respectively. Similarly, the SPECT/CT imaging was performed at 71.84 ± 1.05 h.

A comparison of the normalized cumulated activity and DpA obtained from the planar and hybrid scenarios is presented using the Bland–Altman plot in Figs. 3–7. For each organ and tumor lesion, the mean is offset and suggesting bias as the mean lies above zero. Moreover, variability around the mean is not constant. No trend was observed in relation to the agreement, as data cluster was found more or less in the lower right and most of the organs move upward after passing from left to right.

Organ doses from ^{177}Lu-trastuzumab

The detailed absorbed doses received by organs from a pretherapeutic injection of ^{177}Lu-trastuzumab are discussed here. The mean absorbed dose to heart, lungs, liver, spleen and kidneys was 0.28 ± 0.07, 0.26 ± 0.05, 0.44 ± 0.09, 0.23 ± 0.07 and 0.32 ± 0.11 Gy, respectively, for planar scenario and 0.22 ± 0.06, 0.11 ± 0.02, 0.35 ± 0.06, 0.18 ± 0.05 and 0.24 ± 0.09 Gy, respectively, for hybrid scenario.

The median dose per administered activity of heart, lungs, liver, spleen and kidneys determined by planar scenario was compared to hybrid scenario and found to

Table 2 Patients organ masses (g)

	Heart (g)	Lungs (g)	Liver (g)	Spleen (g)	Kidneys (g)
Mean ± SD	266.18 ± 38.87	598.71 ± 133.74	1638.18 ± 192.68	278.72 ± 72.95	467.27 ± 73.25
50th (25th/75th)	271 (249/279)	579 (467/734)	1587 (1438/1841)	297 (193/331)	458 (427/543)
Range	191–328	452–809	1410–1933	184–389	367–583

Table 3 Normalized cumulated activity of organs and remainder body obtained by Dosimetry Toolkit using planar and hybrid imaging scenarios

	Heart (h)	Lungs (h)	Liver (h)	Spleen (h)	Kidneys (h)	Remainder body (h)
Planar						
Mean ± SD	2.90 ± 0.96	8.13 ± 2.51	20.60 ± 3.49	1.39 ± 0.59	3.15 ± 1.17	63.52 ± 10.80
50th (25th/75th)	3.22 (2.08/3.86)	9.21 (5.22/9.71)	20.16 (15.22/24.78)	1.07 (0.89/1.93)	3.13 (2.34/4.06)	66.41 (55.12/72.67)
Range	0.91–3.96	4.61–12.12	15.22–24.78	0.82–2.54	1.32–4.77	45.18–74
Hybrid						
Mean ± SD	2.31 ± 0.72	5.10 ± 1.84	16.02 ± 2.71	0.93 ± 0.46	2.67 ± 1.11	46.54 ± 8.84
50th (25th/75th)	2.57 (1.58/2.91)	5.24 (3.26/5.88)	15.44 (12.71/18.61)	0.72 (0.67/1.17)	2.49 (1.87/3.41)	46.29 (38.49/55.98)
Range	0.67–2.95	2.14–8.89	12.67–19.32	0.54–1.86	1.11–4.43	35.29–59
*P**	0.003	0.01	0.003	0.003	0.003	0.01

P=significance of difference between planar scenerio and hybrid scenerio (Wilcoxon signed-rank test).

Table 4 Dose per administered activity of organs in planar and hybrid imaging scenarios

	Heart (mGy/MBq)	Lungs (mGy/MBq)	Liver (mGy/MBq)	Spleen (mGy/MBq)	Kidneys (mGy/MBq)	Adrenal (mGy/MBq)	Pancreas (mGy/MBq)	Colon (mGy/MBq)
Planar								
Mean ± SD	0.81 ± 0.19	0.75 ± 0.13	1.26 ± 0.25	0.68 ± 0.22	0.91 ± 0.31	0.18 ± 0.04	0.25 ± 0.22	0.75 ± 0.61
50th (25th/75th)	0.89 (0.71/0.94)	0.75 (0.63/0.81)	1.35 (0.94/1.39)	0.61 (0.58/0.69)	0.91 (0.58/1.16)	0.17 (0.14/0.23)	0.17 (0.11/0.29)	0.58 (0.41/0.67)
Range	0.34–1.02	0.57–1.05	0.88–1.67	0.49–1.31	0.44–1.43	0.12–0.25	0.09–0.75	0.28–2.12
Hybrid								
Mean ± SD	0.63 ± 0.17	0.32 ± 0.06	1.01 ± 0.17	0.53 ± 0.16	0.69 ± 0.24	0.11 ± 0.02	0.09 ± 0.02	0.44 ± 0.28
50th (25th/75th)	0.71 (0.55/0.75)	0.30 (0.28/0.39)	1.07 (0.78/1.14)	0.48 (0.45/0.57)	0.71 (0.40/0.81)	0.10 (0.09/0.14)	0.09 (0.08/0.12)	0.40 (0.29/0.51)
Range	0.20–0.80	0.18–0.41	0.76–1.29	0.38–0.97	0.37–1.20	0.08–0.16	0.06–0.15	0.13–1.04
*P**	0.003	0.01	0.003	0.003	0.003	0.01	0.01	0.01

P=significance of difference between planar scenerio and hybrid scenerio (Wilcoxon signed-rank test).

Fig. 3

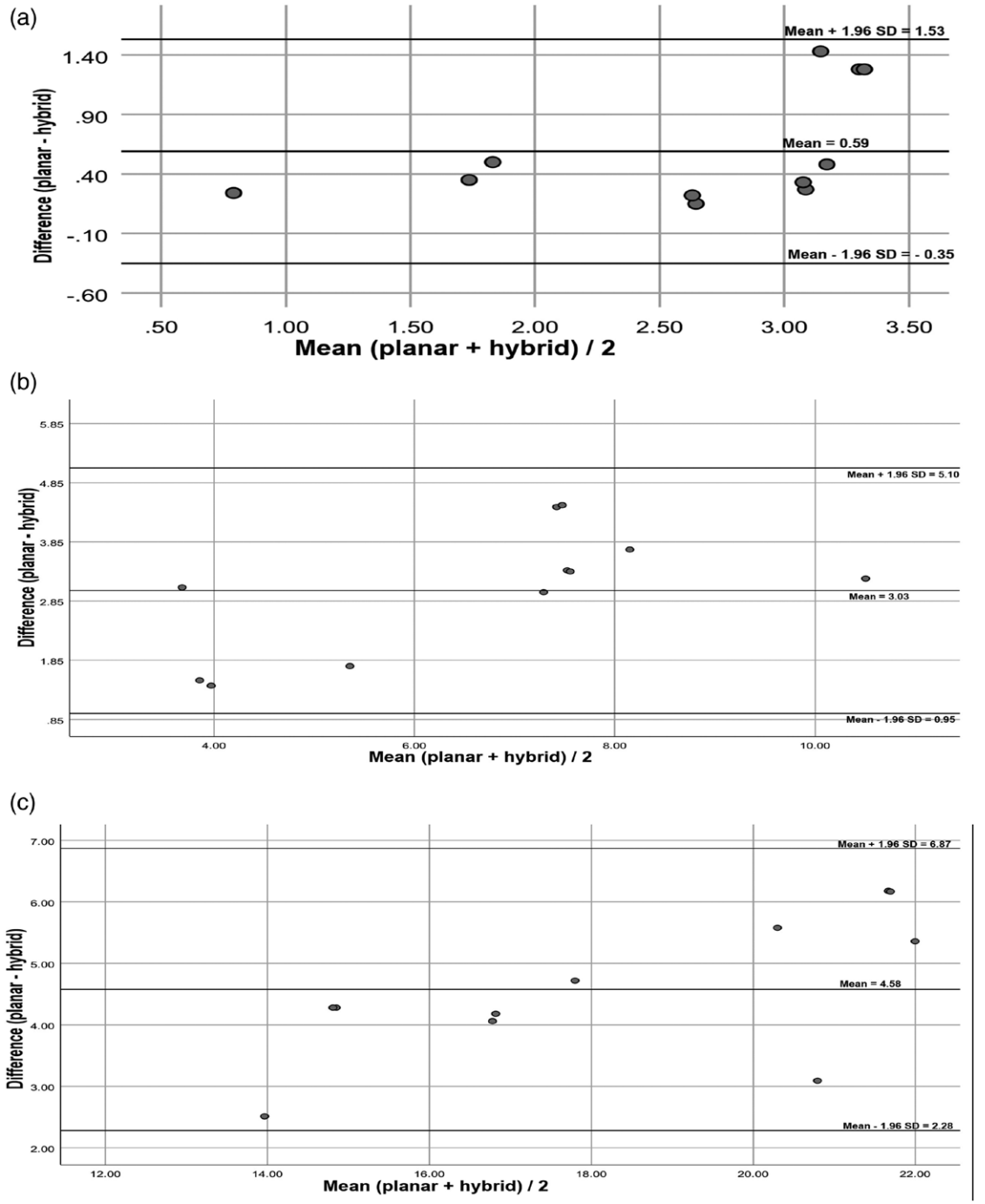

Bland–Altman plots of (a) heart, (b) lung and (c) liver normalized cumulated activity obtained from the planar and hybrid scenarios. The *x*-axis represents the mean of planar and hybrid normalized cumulated activity and the *y*-axis is the difference between planar and hybrid normalized cumulated activity. Midline with numerical values denotes mean differences, whereas the rest two lines lie above and below the mean with values denote 95% confidence interval of the limits of agreement.

be increased by a factor of 1.2 ($P = 0.003$), 2.5 ($P = 0.01$), 1.2 ($P = 0.003$), 1.2 ($P = 0.003$) and 1.2 ($P = 0.003$), respectively.

Estimations for the adrenal, pancreas and colon revealed mean absorbed dose of 0.06 ± 0.01, 0.09 ± 0.09 and 0.26 ± 0.20 Gy, respectively, for the planar scenario and 0.04 ± 0.01, 0.03 ± 0.01 and 0.15 ± 0.09 Gy, for the hybrid scenario. The median dose per administered activity of adrenal, pancreas and colon determined by planar scenario was compared to the hybrid scenario and found

Fig. 4

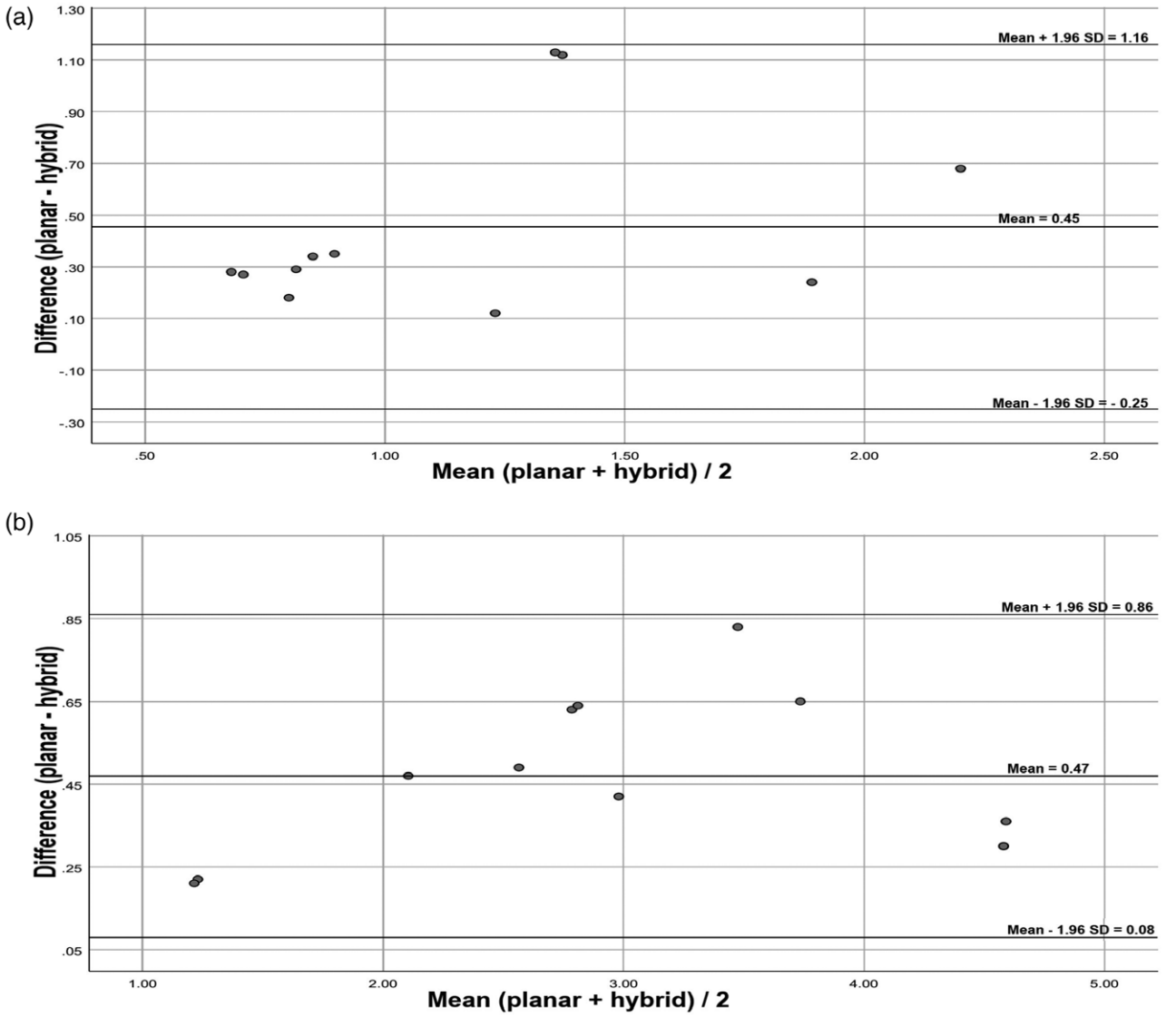

Bland–Altman plots of (a) spleen and (b) kidneys normalized cumulated activity obtained from the planar and hybrid scenarios. The *x*-axis represents the mean of planar and hybrid normalized cumulated activity and the *y*-axis is the difference between planar and hybrid normalized cumulated activity. Midline with numerical values denotes mean differences, whereas the rest two lines lie above and below the mean with values denote 95% confidence interval of the limits of agreement.

to be increased by a factor of 1.7 ($P = 0.01$), 1.9 ($P = 0.01$) and 1.4 ($P = 0.01$), respectively, using multiplanar imaging scenario.

Normalized cumulated activity and dose to tumors

Liver tumor lesions ($n = 10$) were assessed for both scenarios. The details of tumor normalized cumulated activity and DpA are mentioned in Table 5. The mean masses of the tumor were 73 ± 29 g (median = 79 g, range = 21–126 g). The mean absorbed dose for the tumor was 3.66 ± 2.83 and 2.95 ± 2.36 Gy in planar and hybrid scenarios, respectively. The median dose per administered activity of the tumor determined by the planar scenario was compared to the hybrid scenario and found to be increased by a factor of 1.3 ($P = 0.005$).

In both the scenarios, tumor and liver received maximum absorbed dose from ^{177}Lu-trastuzumab. The progressive retention of tracer in the tumor and whole liver is shown in Fig. 8.

Discussion

Over the last few years, radioimmunotherapy developed as a popular treatment option in many diseases [32]. Trastuzumab is the first mAb approved in the treatment of breast cancers and successfully radiolabeled

Fig. 5

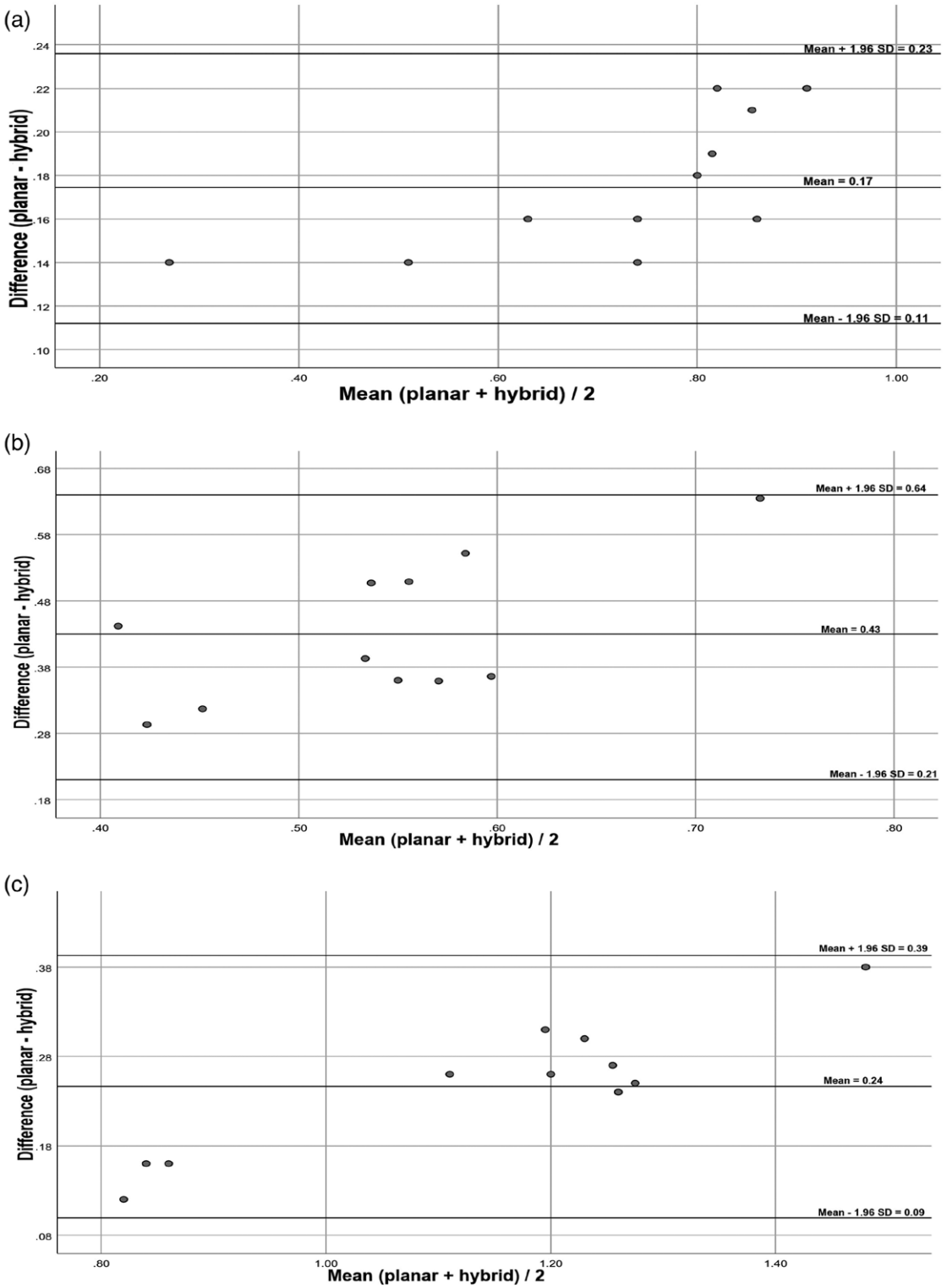

Bland–Altman plots of (a) heart, (b) lung and (c) liver absorbed dose obtained from the planar and hybrid scenarios. The *x*-axis represents the mean of planar and hybrid absorbed doses and the *y*-axis is the difference between planar and hybrid absorbed doses. Midline with numerical values denotes mean differences, whereas the rest two lines lie above and below the mean with values denote 95% confidence interval of the limits of agreement.

Fig. 6

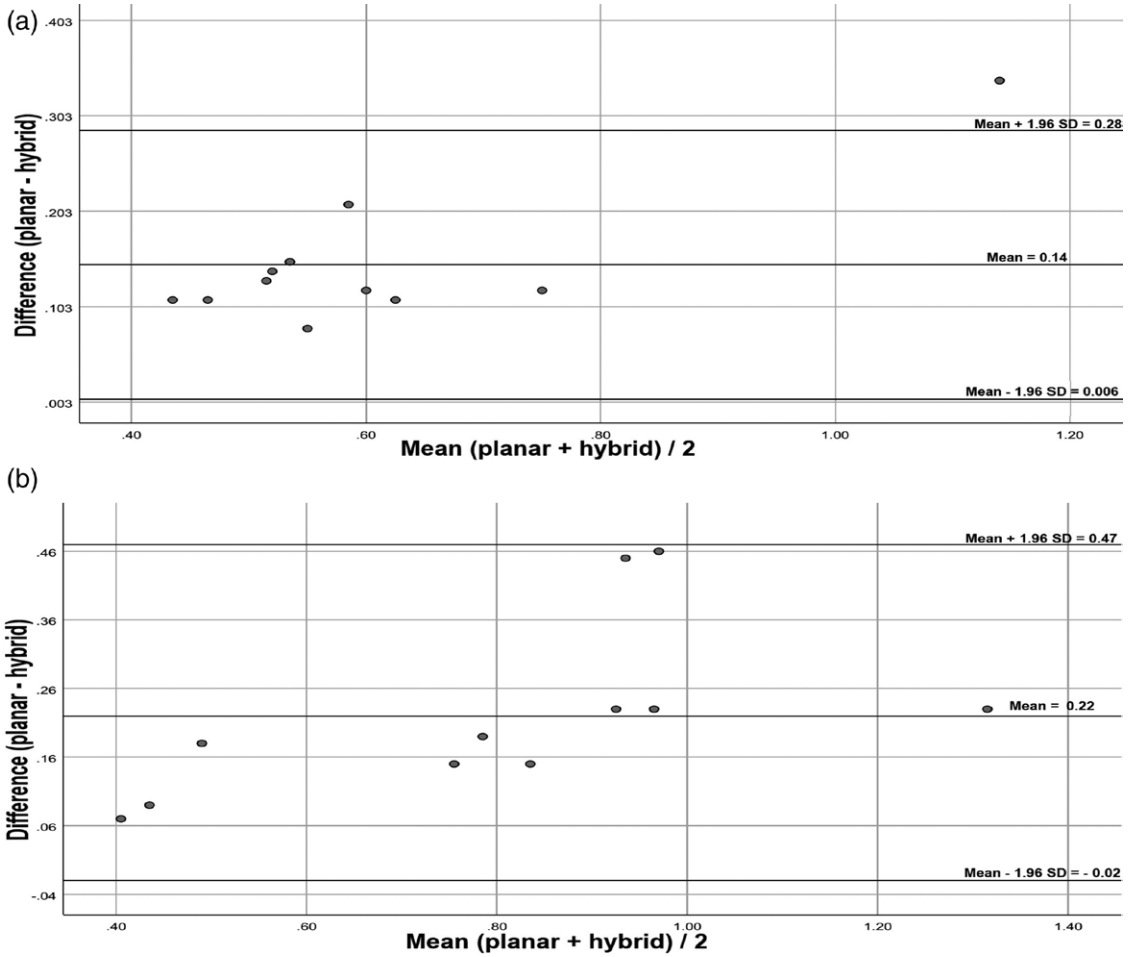

Bland–Altman plots of (a) spleen and (b) kidneys absorbed dose obtained from the planar and hybrid scenarios. The *x*-axis represents the mean of planar and hybrid absorbed doses and the *y*-axis is the difference between planar and hybrid absorbed doses. Midline with numerical values denotes mean differences, whereas the rest two lines lie above and below the mean with values denote 95% confidence interval of the limits of agreement.

with many beta and alpha-emitting isotopes [8,33,34]. However, ^{177}Lu emerged as most popular among all because of its ideal physical characteristics [35]. This is likely the first report demonstrating pretherapeutic dosimetry results in organs and tumor lesions with ^{177}Lu-trastuzumab on breast cancer patients undergoing high-dose radioimmunotherapy.

The basic concept of targeted RNT is to deliver a high radiation dose to target tissue without affecting healthy normal tissue. Unlike external radiotherapy, RNT is more complicated in aspects of dosimetry calculations because of gross variation in organ or tumor uptake amongst patients. To increase the efficacy of RNT treatment, prior knowledge of bio-distribution and organ doses of radiopharmaceutical is important. This can be assessed using the results of pretherapeutic dosimetry [36].

In our study, qualitative observation revealed a high target to nontarget ratio in day 4 to day 7 postadministration of ^{177}Lu-trastuzumab. This is mainly due to high blood pool activity and slower clearance of mAb from circulation [9,37–39]. Metastatic liver sites receive a high absorbed dose compared to other organ systems, makes radioimmunotherapy an effective treatment option. Other authors also reported the potential of trastuzumab radioimmunotherapy in the treatment of *HER2*-positive malignancies [40,41]. In both imaging scenarios, tumor dose was eight times higher as compared to normal liver tissue. Similar to our results, a pre-clinical study also reported six times the higher absorbed dose in the tumor as compared to the normal liver [42]. In the present study, the dose estimation for the tumor in the planar and hybrid scenarios reported an average DpA of 10.22 ± 7.41 and 8.23 ± 6.19 mGy/MBq. Since, most of ^{177}Lu-trastuzumab-based studies are limited to preparation, biodistribution and estimation of uptake in normal organs, no comparable reference dose values were demonstrated [8,9,11,43]. However, the absorbed dose calculated in previous research work with ^{90}Y-trastuzumab

Fig. 7

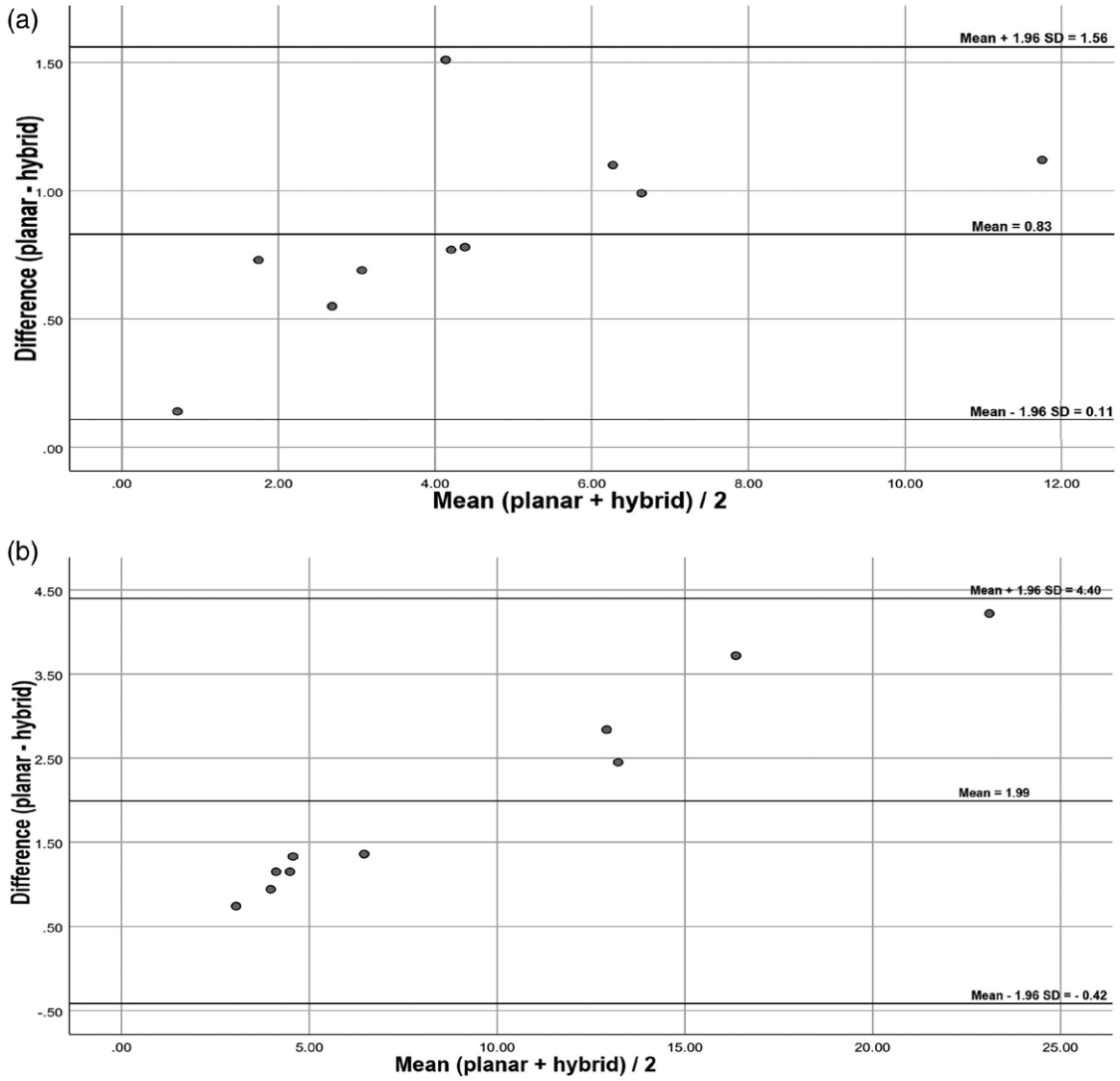

Bland–Altman plots for tumor (a) normalized cumulated activity and (b) absorbed dose obtained from the planar and hybrid scenarios. The *x*-axis represents the mean of planar and hybrid scenarios and the *y*-axis is the difference between planar and hybrid scenarios. Midline with numerical values denotes mean differences, whereas the rest two lines lie above and below the mean with values denote 95% confidence interval of the limits of agreement.

was 15.86 ± 17.32 mGy/MBq [44]. Moreover, the high SD of absorbed dose was reported in our study mainly due to inter-individual variability and heterogeneity in the tumor.

In the present study, the normal biodistribution of ^{177}Lu-trastuzumab was noted in the heart, liver, spleen and kidneys. A similar pattern of distribution has been demonstrated in previous literature [9,39]. However, our dosimetry calculation suggests the liver is a major organ at risk mainly due to higher uptake and slow clearance from the body. The dose estimation for the liver in the planar and hybrid scenarios reported an average DpA of 1.26 ± 0.25 and 1.01 ± 0.17 mGy/MBq. Laforest *et al*, [45] found the liver as a critical organ with an absorbed dose of 1.54 mGy/MBq due to the highest retention of ^{89}Zr-trastuzumab. Study by Wong *et al*. [44] suggested the predicted absorbed dose to be 4.75 ± 0.37 mGy/MBq for the liver with 90Y-trastuzumab. Concerning uptake, various preclinical and clinical studies revealed the highest accumulation of activity in the liver compared to other organs [9,37,46]. On the basis of our results, a maximum threshold dose of 30 Gy in the liver [47] would be attained after an average of four to five treatment cycles with 5.5 GBq injected activity of ^{177}Lu-trastuzumab.

The average DpA calculated for other organs at risk that is, kidneys, heart and spleen in the planar and hybrid scenarios was 0.91 ± 0.31 and 0.69 ± 0.24; 0.81 ± 0.19 and

Table 5 Normalized cumulated activity and dose per administered activity (DpA) of $n=10$ liver tumor lesions in planar and hybrid imaging scenarios

	Tumor	
	Normalized cumulated activity	DpA (mGy/MBq)
Planar		
Mean ± SD	4.97 ± 3.23	10.22 ± 7.41
50th (25th/75th)	4.58 (2.74/6.89)	6.18 (4.62/15.39)
Range	0.78–12.31	3.42–25.22
Hybrid		
Mean ± SD	4.13 ± 3.01	8.23 ± 6.19
50th (25th/75th)	3.6 (2.15/5.82)	4.84 (3.53/12.62)
Range	0.64–11.19	2.68–21
*P**	0.005	0.005

Fig. 8

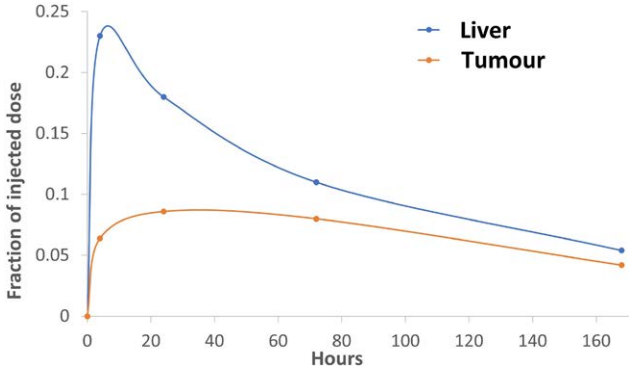

Time-activity curve of entire liver excluding tumor and liver-tumor ROI following injection of ^{177}Lu-trastuzumab across all the patient population. ROI, region of interest.

0.63 ± 0.17 and 0.68 ± 0.22 and 0.53 ± 0.16 mGy/MBq, respectively. Our results are in contrast with the uptake-based findings obtained by authors suggested uptake in kidney, heart and spleen for 4–7 days postinjection of radiolabeled trastuzumab [9,38,39,48]. Meanwhile, a patient-based diagnostic study using ^{68}Ga-DOTA-F(ab0)2-trastuzumab reported highest concentration and mean absorbed dose in kidneys (0.10 mGy/MBq) as compared to liver and heart (0.09 mGy/MBq and 0.07 mGy/MBq) [49]. This is likely due to faster kinetics and clearance of fragmented antibodies from intravascular compartments. Because lung in radioimmunotherapy with ^{177}Lu-trastuzumab are not considered as risk organs, no comparable context values were demonstrated by other authors.

Multi-SPECT/CT scenario provides the most precise results compared to planar and hybrid imaging techniques used in our study. This is mainly due to 3D voxel-based quantification, nonoverlapping 3D organ delineation and attenuation corrected SPECT data [23,50,51]. However, the major drawback of multi-SPECT/CT scenario is highly time consuming and complex VOI definition [23]. Moreover, the patient receives additional CT exposure from each sequential acquisition. In the present study, we observed that planar scenario was rapid and simple to perform mainly due to simple image processing and ROI definition. The measured DpAs from 2D planar scenario was relatively higher in all organs and tumor lesions compared to the hybrid scenario. The maximum difference in median DpA was noted in the lungs due to overlapping liver counts in the lower lobe of the right lung. The overestimation of doses in 2D scenario is mostly caused by higher normalized cumulated activity related to overlapping organ segmentation with ROIs and the use of organ and body thickness-based weighting factors for background correction of organs embedded in background activity [23,50,51]. The integration of multiplanar scans with single SPECT/CT in the hybrid scenario is a more convenient and less time-consuming method than a multi SPECT/CT scenario. In the hybrid scenario, organ VOI were drawn either in SPECT or CT images to avoid overlapping of organ structures before they launched onto multiplanar whole-body images for the correction of superimposed regions. However, the major limitation of the hybrid scenario is an extrapolation of homogenously distributed VOI activity onto the overlapped planar whole-body regions with nonuniform activity distribution [23,26].

Our study also has some limitations. Our dosimetric analysis and comparison were limited to vendor-specific software which couldn't fit data bi-exponentially. Further work needs to be performed that includes a comparison of software products supplied by different vendors. We did not carry out multi-SPECT/CT-based dosimetry for comparison because of their reported multiplicities. Moreover, the cross radiation in tumor spheres has not been examined.

On the basis of the dosimetric assessment, we concluded that radioimmunotherapy with ^{177}Lu-trastuzumab is well tolerated to be implemented in routine clinical practice against *HER2* positive metastatic breast cancer. This pilot study shows the liver as an organ at risk in ^{177}Lu-trastuzumab radioimmunotherapy. Also, the hybrid imaging scenario demonstrated significantly lower absorbed doses in organs and tumors compared to the multiplanar method. Further studies based on a large number of patients are needed to validate our study results.

Acknowledgements

We would like to thank all staff and students of the Nuclear Medicine Department, TMH, Mumbai for technical and clinical support.

Conflicts of interest

There are no conflicts of interest.

References

1 James R, Thriveni K, Krishnamoorthy L, Deshmane V, Bapsy PP, Ramaswamy G. Clinical outcome of adjuvant endocrine treatment according to Her-2/neu status in breast cancer. *Indian J Med Res* 2011; **133**:70–75.

2 Ross JS, Fletcher JA, Linette GP, Stec J, Clark E, Ayers M, *et al*. The Her-2/neu gene and protein in breast cancer 2003: biomarker and target of therapy. *Oncologist* 2003; **8**:307–325.
3 Goldenberg DM. Radiolabelled monoclonal antibodies in the treatment of metastatic cancer. *Curr Oncol* 2007; **14**:39–42.
4 Metro G, Mottolese M, Fabi A. HER-2-positive metastatic breast cancer: trastuzumab and beyond. *Expert Opin Pharmacother* 2008; **9**:2583–2601.
5 Rasaneh S, Rajabi H, Babaei MH, Daha FJ. 177Lu labeling of Herceptin and preclinical validation as a new radiopharmaceutical for radioimmunotherapy of breast cancer. *Nucl Med Biol* 2010; **37**:949–955.
6 Milenic DE, Garmestani K, Brady ED, Albert PS, Ma D, Abdulla A, *et al*. Alpha-particle radioimmunotherapy of disseminated peritoneal disease using a (212)Pb-labeled radioimmuno conjugate targeting HER2. *Cancer Biother Radiopharm* 2005; **20**:557–568.
7 Chen KT, Lee TW, Lo JM. *In vivo* examination of (188)Re(I)-tricarbonyl-labeled trastuzumab to target HER2-overexpressing breast cancer. *Nucl Med Biol* 2009; **36**:355–361.
8 Rasaneh S, Rajabi H, Babaei MH, Daha FJ, Salouti M. Radiolabeling of trastuzumab with 177Lu via DOTA, a new radiopharmaceutical for radioimmunotherapy of breast cancer. *Nucl Med Biol* 2009; **36**:363–369.
9 Bhusari P, Vatsa R, Singh G, Parmar M, Bal A, Dhawan DK, *et al*. Development of Lu-177-trastuzumab for radioimmunotherapy of HER2 expressing breast cancer and its feasibility assessment in breast cancer patients. *Int J Cancer* 2017; **140**:938–947.
10 Kameswaran M, Pandey U, Gamre N, Sarma HD, Dash A. Preparation of 177Lu-trastuzumab injection for treatment of breast cancer. *Appl Radiat Isot* 2019; **148**:184–190.
11 Hermanto S, Haryuni RD, Ramli M, Mutalib A, Hudiyono S. Synthesis and stability test of radioimmunoconjugate 177Lu-DOTA-F (ab0) 2-trastuzumab for theranostic agent of HER2 positive breast cancer. *J Radiat Res Appl Sci* 2016; **9**:441–448.
12 Hindorf C, Glatting G, Chiesa C, Lindén O, Flux G; EANM Dosimetry Committee. EANM Dosimetry Committee guidelines for bone marrow and whole-body dosimetry. *Eur J Nucl Med Mol Imaging* 2010; **37**:1238–1250.
13 Lassmann M, Chiesa C, Flux G, Bardiès M; EANM Dosimetry Committee. EANM Dosimetry Committee guidance document: good practice of clinical dosimetry reporting. *Eur J Nucl Med Mol Imaging* 2011; **38**:192–200.
14 Bolch WE, Eckerman KF, Sgouros G, Thomas SR. MIRD pamphlet No. 21: a generalized schema for radiopharmaceutical dosimetry – standardization of nomenclature. *J Nucl Med* 2009; **50**:477–484.
15 Pauwels S, Barone R, Walrand S, Borson-Chazot F, Valkema R, Kvols LK, *et al*. Practical dosimetry of peptide receptor radionuclide therapy with (90) Y-labeled somatostatin analogs. *J Nucl Med* 2005; **46** (Suppl 1):92S–98S.
16 Garkavij M, Nickel M, Sjögreen-Gleisner K, Ljungberg M, Ohlsson T, Wingårdh K, *et al*. 177Lu-[DOTA0,Tyr3] octreotate therapy in patients with disseminated neuroendocrine tumors: analysis of dosimetry with impact on future therapeutic strategy. *Cancer* 2010; **116**:1084–1092.
17 Frey EC, Humm JL, Ljungberg M. Accuracy and precision of radioactivity quantification in nuclear medicine images. *Semin Nucl Med* 2012; **42**:208–218.
18 Cremonesi M, Botta F, Di Dia A, Ferrari M, Bodei L, De Cicco C, *et al*. Dosimetry for treatment with radiolabelled somatostatin analogues. A review. *Q J Nucl Med Mol Imaging* 2010; **54**:37–51.
19 Sandström M, Garske U, Granberg D, Sundin A, Lundqvist H. Individualized dosimetry in patients undergoing therapy with (177)Lu-DOTA-D-Phe (1)-Tyr (3)-octreotate. *Eur J Nucl Med Mol Imaging* 2010; **37**:212–225.
20 Berker Y, Goedicke A, Kemerink GJ, Aach T, Schweizer B. Activity quantification combining conjugate-view planar scintigraphies and SPECT/CT data for patient-specific 3-D dosimetry in radionuclide therapy. *Eur J Nucl Med Mol Imaging* 2011; **38**:2173–2185.
21 Dewaraja YK, Frey EC, Sgouros G, Brill AB, Roberson P, Zanzonico PB, Ljungberg M. MIRD pamphlet No. 23: quantitative SPECT for patient-specific 3-dimensional dosimetry in internal radionuclide therapy. *J Nucl Med* 2012; **53**:1310–1325.
22 Lehnert W, Schmidt K, Kimiaei S, Meyer T, Bronzel M, Kluge A. Impact of modality (2D planar, 2D/3D hybrid, 3D SPECT) on kidneys absorbed dose in 177Lu-based PRRT. *J Nucl Med* 2018; **59** (Suppl 1):391.
23 Kupitz D, Wetz C, Wissel H, Wedel F, Apostolova I, Wallbaum T, *et al*. Software-assisted dosimetry in peptide receptor radionuclide therapy with 177Lutetium-DOTATATE for various imaging scenarios. *PLoS One* 2017; **12**:e0187570.
24 Sundlöv A, Sjögreen-Gleisner K, Svensson J, Ljungberg M, Olsson T, Bernhardt P, Tennvall J. Individualised 177Lu-DOTATATE treatment of neuroendocrine tumours based on kidney dosimetry. *Eur J Nucl Med Mol Imaging* 2017; **44**:1480–1489.
25 Roth D, Gustafsson J, Sundlöv A, Sjögreen Gleisner K. A method for tumor dosimetry based on hybrid planar-SPECT/CT images and semiautomatic segmentation. *Med Phys* 2018; **45**:5004–5018.
26 GE Healthcare. Organ dose estimates for radio-isotope therapy treatment planning purposes. Dosimetry toolkit package. White Paper. 2011.
27 Buijs WC, Massuger LF, Claessens RA, Kenemans P, Corstens FH. Dosimetric evaluation of immunoscintigraphy using indium-111-labeled monoclonal antibody fragments in patients with ovarian cancer. *J Nucl Med* 1992; **33**:1113–1120.
28 Stabin M, Farmer A. OLINDA/EXM 2.0: the new generation dosimetry modeling code. *J Nucl Med* 2012; **53** (Suppl 1):585.
29 Park S, Lee JK, Kim JI, Lee YJ, Lim YK, Kim CS, Lee C. *In vivo* organ mass of Korean adults obtained from whole-body magnetic resonance data. *Radiat Prot Dosimetry* 2006; **118**:275–279.
30 Howard DM, Kearfott KJ, Wilderman SJ, Dewaraja YK. Comparison of I-131 radioimmunotherapy tumor dosimetry: unit density sphere model versus patient-specific Monte Carlo calculations. *Cancer Biother Radiopharm* 2011; **26**:615–621.
31 Grimes J, Celler A. Comparison of internal dose estimates obtained using organ-level, voxel S value, and Monte Carlo techniques. *Med Phys* 2014; **41**:092501.
32 O'Donnell RT, DeNardo GL, Kukis DL, Lamborn KR, Shen S, Yuan A, *et al*. 67Copper-2-iminothiolane-6-[p-(bromoacetamido)benzyl-TETA-Lym-1 for radioimmunotherapy of non-Hodgkin's lymphoma. *Clin Cancer Res* 1999; **5** (10 Suppl):3330s–3336s.
33 Crow DM, Williams L, Colcher D, Wong JY, Raubitschek A, Shively JE. Combined radioimmunotherapy and chemotherapy of breast tumors with Y-90-labeled anti-Her2 and anti-CEA antibodies with taxol. *Bioconjug Chem* 2005; **16**:1117–1125.
34 Luo TY, Tang IC, Wu YL, Hsu KL, Liu SW, Kung HC, *et al*. Evaluating the potential of 188Re-SOCTA-trastuzumab as a new radioimmunoagent for breast cancer treatment. *Nucl Med Biol* 2009; **36**:81–88.
35 Vallabhajosula S, Kuji I, Hamacher KA, Konishi S, Kostakoglu L, Kothari PA, *et al*. Pharmacokinetics and biodistribution of 111In- and 177Lu-labeled J591 antibody specific for prostate-specific membrane antigen: prediction of 90Y-J591 radiation dosimetry based on 111In or 177Lu? *J Nucl Med* 2005; **46**:634–641.
36 Thierens HM, Monsieurs MA, Bacher K. Patient dosimetry in radionuclide therapy: the whys and the wherefores. *Nucl Med Commun* 2005; **26**:593–599.
37 Ramli M, Humani TS, Rustendi CT, Subur M, Karyadi SA. Preparation, stability and biodistribution studies of177Lu-DOTA-trastuzumab, a potential radiopharmaceutical for radioimmunotherapy of breast cancer. In International Conference on Biomass Production Proceedings, School of Life Sciences and Technology, Bandung Institute of Technology 2009; 25e26 November, ISBN 978-602-96488-0-5.
38 Dijkers EC, Oude Munnink TH, Kosterink JG, Brouwers AH, Jager PL, de Jong JR, *et al*. Biodistribution of 89Zr-trastuzumab and PET imaging of HER2-positive lesions in patients with metastatic breast cancer. *Clin Pharmacol Ther* 2010; **87**:586–592.
39 Tamura K, Kurihara H, Yonemori K, Tsuda H, Suzuki J, Kono Y, *et al*. 64Cu-DOTA-trastuzumab PET imaging in patients with HER2-positive breast cancer. *J Nucl Med* 2013; **54**:1869–1875.
40 Choi S, Lim I, Kim BI, Lim SM. Therapeutic efficacy of I-131 trastuzumab radio- immunotherapy in HER2 positive tumor is improved after the combination of lanatoside C. *J Nucl Med* 2017; **58** (Suppl 1):687.
41 Kawashima H. Radioimmunotherapy: a specific treatment protocol for cancer by cytotoxic radioisotopes conjugated to antibodies. *Scientificworldjournal* 2014; **2014**:492061.
42 Rasaneh S, Rajabi H, Akhlaghpoor S, Sheybani S. Radioimmunotherapy of mice bearing breast tumors with 177Lu-labeled trastuzumab. *Turk J Med Sci* 2013; **42**:1292–1298.
43 Spector NL, Blackwell KL. Understanding the mechanisms behind trastuzumab therapy for human epidermal growth factor receptor 2-positive breast cancer. *J Clin Oncol* 2009; **27**:5838–5847.
44 Wong JY, Raubitschek A, Yamauchi D, Williams LE, Wu AM, Yazaki P, *et al*. A pretherapy biodistribution and dosimetry study of indium-111-radiolabeled trastuzumab in patients with human epidermal growth factor receptor 2-overexpressing breast cancer. *Cancer Biother Radiopharm* 2010; **25**:387–394.
45 Laforest R, Lapi SE, Oyama R, Bose R, Tabchy A, Marquez-Nostra BV, *et al*. [89Zr]Trastuzumab: evaluation of radiation dosimetry, safety, and optimal

imaging parameters in women with HER2-positive breast cancer. *Mol Imaging Biol* 2016; **18**:952–959.
46 Kwon LY, Scollard DA, Reilly RM. 64Cu-labeled Trastuzumab Fab-PEG24-EGF radioimmunoconjugates bispecific for HER2 and EGFR: pharmacokinetics, biodistribution, and tumor imaging by PET in comparison to monospecific agents. *Mol Pharm* 2017; **14**:492–501.
47 Emami B, Lyman J, Brown A, Coia L, Goitein M, Munzenrider JE, *et al*. Tolerance of normal tissue to therapeutic irradiation. *Int J Radiat Oncol Biol Phys* 1991; **21**:109–122.
48 Abbas N, Bruland ØS, Brevik EM, Dahle J. Preclinical evaluation of 227Th-labeled and 177Lu-labeled trastuzumab in mice with HER-2-positive ovarian cancer xenografts. *Nucl Med Commun* 2012; **33**:838–847.
49 Beylergil V, Morris PG, Smith-Jones PM, Modi S, Solit D, Hudis CA, *et al*. Pilot study of 68Ga-DOTA-F(ab')2-trastuzumab in patients with breast cancer. *Nucl Med Commun* 2013; **34**:1157–1165.
50 He B, Frey EC. The impact of 3D volume of interest definition on accuracy and precision of activity estimation in quantitative SPECT and planar processing methods. *Phys Med Biol* 2010; **55**:3535–3544.
51 King M, Farncombe T. An overview of attenuation and scatter correction of planar and SPECT data for dosimetry studies. *Cancer Biother Radiopharm* 2003; **18**:181–190.